

Surface Modification of Aluminum Alloy 6061 for Bipolar Plate Application: Adhesion Characteristics and Corrosion Resistance

A. G. González Gutiérrez¹, P.J. Sebastian^{1,*}, L. Magallón Cacho¹, E. Borja Arco²,
J. Campos¹, Agustín Baron¹

¹ Instituto de Energías Renovables-UNAM, 62580, Temixco, Morelos. México

² Facultad de Química-UNAM, Av Universidad 3000, 04510, C.U. Ciudad de México, Mexico

*E-mail: sjp@ier.unam.mx

Received: 2 April 2017 / Accepted: 30 August 2017 / Published: 6 March 2018

Surface modification studies on aluminum alloy 6061 (AA6061) to improve the surface properties of metallic bipolar plates in fuel cells are presented in this work. The surface of AA6061 was treated first by the electroless process to get a Ni-P coating (AA6061/Ni-P), after that a gold layer was coated by PVD on the modified surface (AA6061/Ni-P/Au). The chemical composition and the roughness variation of the surface during the electroless process were determined by energy-dispersive spectroscopy analysis (EDS) and profilometry respectively. According to XRD studies a solid solution between aluminum and Ni-P interface was formed, improving the adherence of Au on the surface. The corrosion studies of bipolar metal plates were carried out with a potentiostat/galvanostat (Solartron 1287) and a PC with CorreWare software, observing a better corrosion resistance value for AA6061/Ni-P/Au ($5.21 \mu\text{A cm}^{-2}$) compared to bare AA6061 ($51 \mu\text{A cm}^{-2}$). The open circuit potential was measured during 4 hours simulating the anodic and cathodic environments and the best performance was observed for AA6061/Ni-P/Au for both environments.

Keywords: AA6061, bipolar plate, electroless deposition, corrosion resistance, PEMFC.

1. INTRODUCTION

The polymer electrolyte membrane fuel cell (PEMFC) is an electrochemical device that converts chemical energy of a fuel into electrical energy through a redox reaction, whose only by-products are water and heat. This kind of device presents efficient operation, high energy density, modular characteristics, low-temperature operation ($\approx 80 \text{ }^\circ\text{C}$) and zero emissions (when hydrogen fuel is used). The PEMFC is an attractive candidate for applications in propulsion engines and portable devices. PEMFC consists of three main components: membrane electrode assembly (MEAs), bipolar plates and sealing materials. The bipolar plates (BP) are the main components, which connect the cells electrically, provide structure and support to the stack, distribute uniformly the reactive gases, expel

heat efficiently and evacuate water from the cathode, but have to resist the corrosion. The BPs are generally constructed of graphite, material that has a good electrical conductivity and corrosion resistance, however represents 80% of the total weight and 45% of the cost of the cell [1, 2]. Furthermore, graphite is permeable to gases, has low resistance to impacts and vibrations, these disadvantages make it inappropriate for its use in a fuel cell stack and also represents expensive manufacturing costs.

On the other hand, metals offer better mechanical stability than graphite. The options for machining channels are diverse: casting, stamping or computer numerical control (CNC). The use of metallic bipolar plates in fuel cells provides at least 22 % saving in hydrogen consumption in comparison to graphite [3]. The weight, volume and cost of a fuel cell can be significantly reduced by improving the configuration, flow channel design and use of alternative materials [4]. The use of an alternative material (aluminum) to substitute graphite plate is proposed in this work. This material is malleable, has low density and is of low cost. In addition, aluminum also possesses bulk corrosion resistance [5].

The effects of aluminum-coated and graphite bipolar plates on the fuel cell efficiency and durability has been reported [6], the results showed that aluminum-coated plates achieved higher efficiencies and durability than the graphite plates. The surface oxide formed on aluminum-coated plate reduces the corrosion resistance and does not allow good electrical contact between the MEA and the aluminum bipolar plate. Aluminum and its alloys are susceptible to corrosion; besides aluminum coatings have poor adhesion due to the oxide layer formed on its surface. A surface treatment is necessary to obtain good adhesion of any coating [7]. Researches on the use of coated bipolar plates have not focused on the understanding of the processes that take place during coating. However, the understanding of this process will optimize the performance or at least allows predicting it. Different aluminum alloys (AA5052, AA5251, AA3004, AA105) coated with nickel have been reported in the literature [8, 9, 10, 11] for BP applications. These alloys were used because they have lower impurities and the coating process can be controlled. They also showed that the quality of the deposit depends on the type of aluminum alloy. Moreover, El-Enin and co-workers reported the use of 1050 aluminum alloy [12], which was coated with Ni-Co, Ni-Fe-Co, Ni-Mo-Fe and Ni-Mo-Fe-Cr. The best coating was obtained with Ni-Mo-Fe- Cr with a corrosion rate of 2.8 μm per year (15 μm per year is reported for graphite).

Electroless process for nickel coatings produce deposits having microcrystalline, amorphous or fully crystalline nature over a wide range of compositions [13]. Besides, it has a wide range of commercial applications mainly due to advantages such as corrosion resistance, adaptability for uniform coating on complex shapes, etc. In this work the details of physico-chemical treatments that enable a gold coating on aluminum alloy (AA6061) to protect it against corrosion are shown.

2. EXPERIMENTAL DETAILS

2.1. Electroless Process

The surface of AA6061 plate ($A = 1 \text{ cm}^2$) was polished with 600-2000 grit SiC paper in a

Metaserv 300 polisher BUEHLER with constant water flow. After that, it was cleaned with acetone for quick drying and degreasing. Electroless nickel (EN) plating was done by the catalytic reduction of nickel ions employing some reducing agent. To achieve a better adhesion with another material on the aluminum surface, the oxide layer must be removed first [12, 14]. For this purpose the AA6061 alloy plate was immersed in a bath of 0.3 mol L^{-1} NaOH for different periods (pickling process). In the second step, the zincating process was conducted placing a piece of aluminum plate in a solution of 10 g L^{-1} ZnO + 100 g L^{-1} NaOH for different periods. The final step was to place the AA6061 alloy plate in a commercial nickel solution during 10 minutes (Ni-P). The pickling and zincating process were conducted for different periods: 1, 2, 3, 4, 5 and 10 minutes.

To improve the adhesion of nickel coating on aluminum, the AA6061/Ni-P plates were heated up to $500 \text{ }^\circ\text{C}$ under constant flow of nitrogen during 1 hour in a tubular furnace, then the plates were cooled inside the furnace in the same atmosphere to avoid oxide formation. Finally, the AA6061/Ni-P plates were coated with gold (AA6061/Ni-P/Au) by sputtering in a Blazer BAE 250 system in the presence of Argon gas, maintaining the vacuum in the chamber at 1.6×10^{-4} mBar and gas pressure at 5.4×10^{-2} mBar. The current during the deposition was maintained at 60 mA during 2 minutes.

2.2 Physicochemical Characterization

The chemical composition (EDS) and the morphology (SEM) of the plates were characterized using a S-5500 HITACHI system. For XRD studies, a Rigaku DMAX/2200 diffractometer with Cu $K\alpha$ radiation of wavelength 1.5406 \AA was used. The roughness was measured with an Ambios-XP200 profilometer.

2.3 Electrochemical Measurements

The corrosion test was done simulating the aggressive PEMFC environment with an exposed area of 1 cm^2 . The electrochemical studies were carried out at room temperature in a conventional electrochemical cell with a mercury sulphate electrode ($\text{Hg}/\text{Hg}_2\text{SO}_4/0.5 \text{ mol L}^{-1} \text{ H}_2\text{SO}_4$ (MSE) as reference electrode ($\text{MSE} = 0.680 \text{ V/NHE}$) and a graphite rod as counter electrode. The potentials were referred to normal hydrogen electrode (NHE). The $0.5 \text{ mol L}^{-1} \text{ H}_2\text{SO}_4$ solution used as electrolyte was prepared with 98% sulphuric acid (J.T. Baker) and deionized water ($18.2 \text{ M}\Omega\text{cm}$). A potentiostat/galvanostat (Solartron 1287) and a PC with Corre Ware software were used for the electrochemical measurements. AA6061 and AA6061/Ni-P/Au plates were used as working electrodes.

The open circuit potential was measured in both atmospheres during 4 hours under bubbling hydrogen and oxygen to simulate the fuel cell environment. A scanning rate of 2 mV s^{-1} was chosen for cyclic sweep voltammetry studies (-300 to 300 mV vs OCP). The Tafel plots were used to determine the corrosion current density and potential using autotafel fit of the Solartron program.

3. RESULTS AND DISCUSSION

3.1 Chemical Composition (EDS)

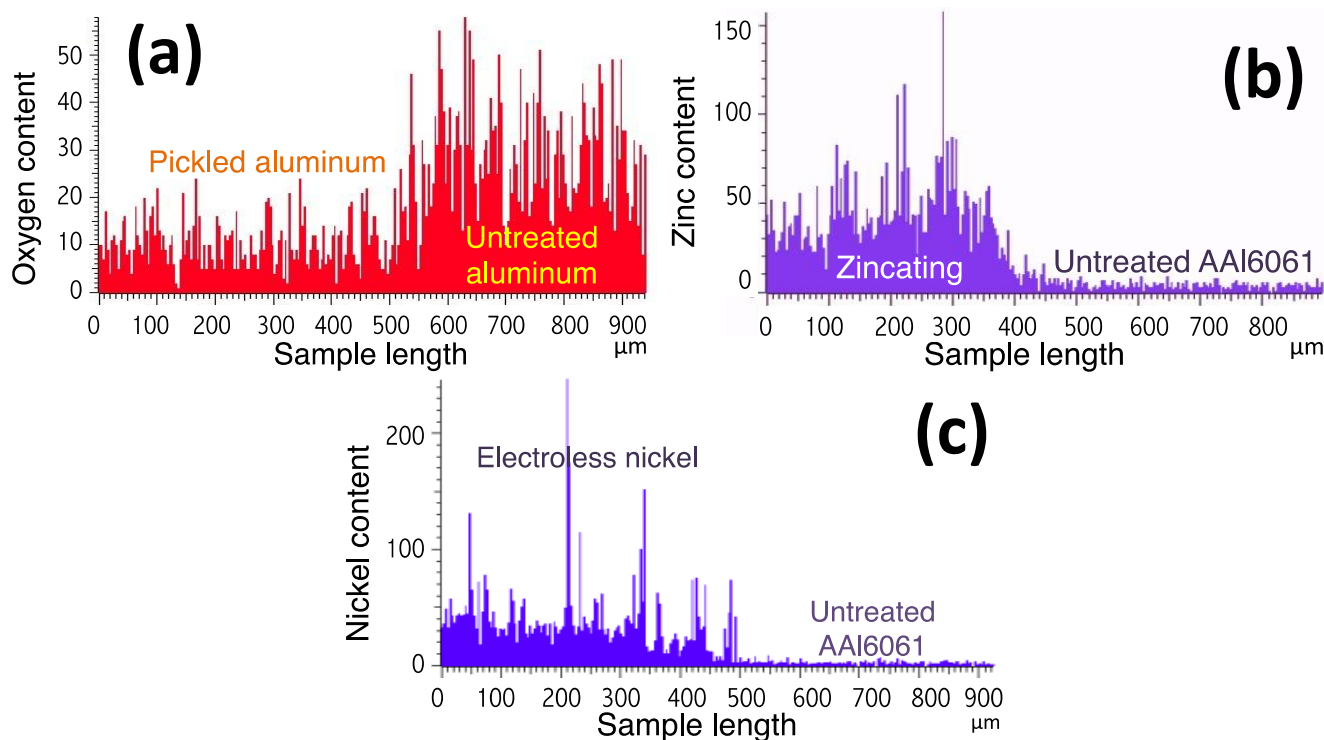


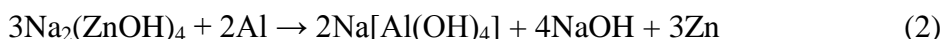
Figure 1. Energy dispersive X-ray patterns of AA6061 alloy after (a) pickling process, (b) zincating process and (c) electroless nickel process (AA6061/Ni-P)

Table 1. Chemical composition of AA6061 alloy during the electroless process determined by EDS.

Element	Bare AA6061		AA6061 pickling		AA6061 Zincating		AA6061 Ni-P	
	Wt.%	Atomic %	Wt.%	Atomic %	Wt.%	Atomic %	Wt.%	Atomic %
Al	63.58	51.94	79.60	74.98	62.41	50.40	68.02	60.42
O	27.07	37.30	11.52	18.30	20.17	27.46	10.69	16.02
Zn	-	-	-	-	3.01	1.00	0.33	0.12
Ni	-	-	-	-	-	-	5.30	2.16
P	-	-	-	-	-	-	4.85	3.75
Other	9.35	10.76	8.88	6.72	14.41	21.41	10.81	17.53

Table 1 shows the chemical composition of the bare AA6061 plate and with electroless treatment and fig. 1 their respective energy dispersive X-ray patterns. It can be observed that AA6061 plate without treatment shows the highest oxygen wt.% value. However, once the pickling of the bare AA6061 plate was carried out the oxygen composition (wt.%) decreased more than 50% because the oxide layer has been eliminated (eq. 1), which favors the electroless process. On the other hand, having carried out the zincating process, the presence of Zn is observed, which was deposited on the AA6061

plate surface (eq. 2) through a galvanic displacement reaction [15, 7, 16]. The zinc layer prevents oxidation of aluminum and promotes the nucleation of nickel [17].



Finally, it can be observed the presence of Ni and P after having deposited it on the Zn layer, with a low oxygen wt.% value.

The zinc coating process is still the most employed for the preparation of aluminum surfaces, however it is possible to include other elements to accelerate the process of nucleation. Recent studies suggest that it is necessary to include more than one procedure prior to the deposition of Ni-P at low temperatures [18]. In this work it was possible to make the deposit at low temperature by controlling the roughness and zinc content.

3.2 Roughness Variation

The roughness on metallic bipolar plates must be minimum ($\approx 2 \mu\text{m}$) to improve the contact and reduce the mass transfer resistances. A high roughness could generate galvanic couples and promote the corrosion. Another effect is the decrease of the hydrophobicity of bipolar plates and the gas mass transfer ability in the fuel cell [19].

The effect of time on the roughness in each chemical bath during the electroless process was studied (fig. 2). In the aluminum pickling both the roughness and depth (wear) increased linearly with time upto 5 minutes (fig. 2a). However, at 10 minutes only the roughness decreased, while the depth increased considerably (table 2). The alkaline bath resulted in the wear process, the aluminum base wearred $\approx 0.78 \mu\text{m}$ per minute.

Table 2. Variation of roughness and depth with time after pickling and zincating processes.

Time (min)	Pickling		Zincating	
	Depth/ μm	Ra/ nm	Depth/ μm	Ra/ nm
0	0	58.70	0	0
1	0.78	97.10	2.71	93.70
2	1.40	107.00	2.51	166.16
3	2.22	117.00	3.64	205.54
4	2.94	136.04	2.06	218.53
5	4.56	157.06	1.38	241.36
10	10.07	152.01	-	-

Fig. 2b shows the results of depth and roughness after applying the zincating process from 1 to 10 minutes. The roughness increased linearly with time. However, the depth remained constant up to 3 minutes, but at 4 minutes the depth increased slightly and at 5 minutes it decreased significantly. This effect is observed because the zinc layer is formed on AA6061 alloy surface. The zincating was studied upto 5 minutes only because the thickness of the zinc layer became unstable.

In fig. 2c shows the roughness of electroless nickel coating without and with heat treatment. The roughness decreased by giving a heat treatment after electroless process, from 143.93 nm (without heat treatment) to 120.11 nm (with heat treatment). This value was reduced due to compacting suffered in the material by diffusion at the interface between aluminum and nickel [20].

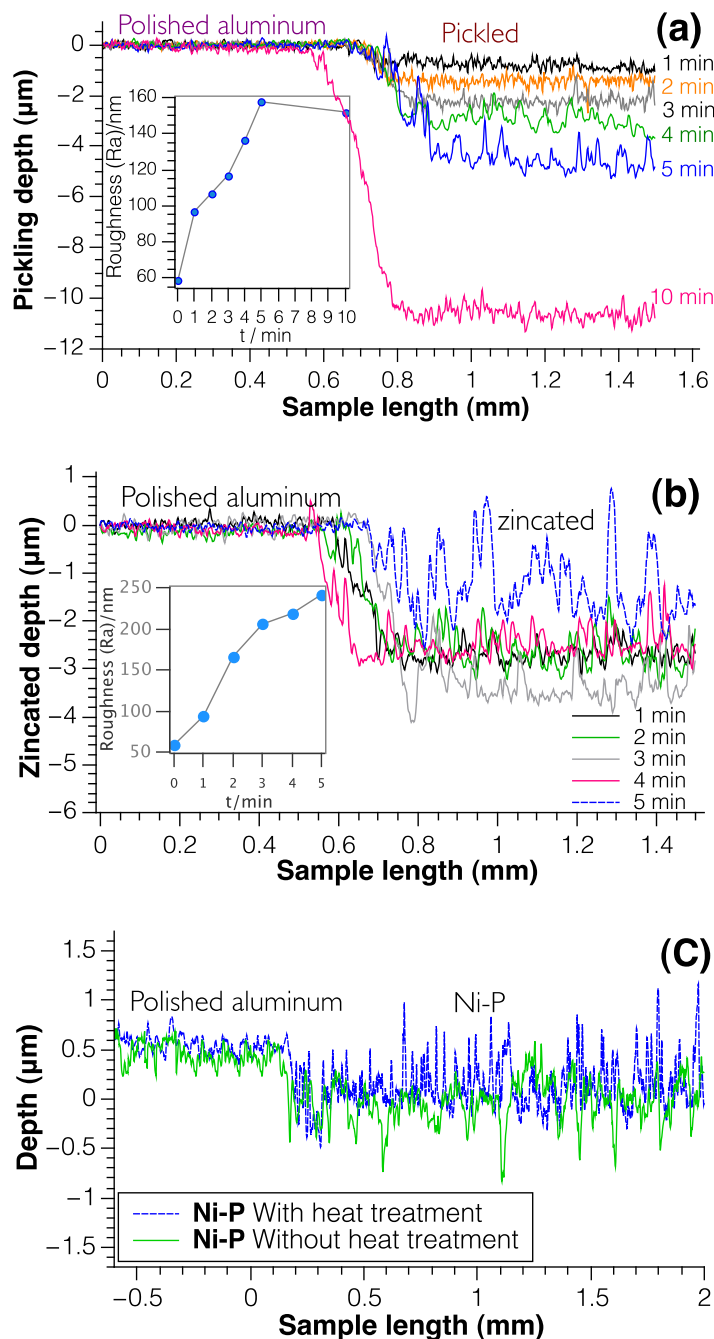


Figure 2. Variation of roughness at different times (a) Pickled surface, (b) Zincating on aluminum, (c) electroless nickel coating with and without heat treatment.

Court et al. [21] conducted the pre-treatment monitoring of aluminum using zincating before nickel electroless and concluded that a complete coverage of the surface by Zn is necessary. In this

work it was found that there is an effect of zincating time. Before 3 minutes the deposit is not formed and after 5 minutes the zinc layer is very thick and loses stability. It has low adhesion and the nickel electroless deposit cannot be possible, in addition the roughness increased.

3.3 X-Ray Diffraction Analysis

Figure 3 shows the X-ray diffraction patterns of AA6061 alloy, Ni-P and Au coated layer on AA6061/Ni-P. All the patterns showed four characteristic peaks of aluminum diffracted at 38.47° , 44.73° , 65.13° and 78.22° . Fig. 3b shows the AA6061/Ni-P diffractogram without heat treatment, where the crystallographic peaks of aluminum are less intense and broader with respect to AA6061 alloy (fig. 3a). Nickel-phosphorus coating is amorphous, so semi-crystalline and amorphous peaks on aluminum alloy are observed. By increasing the content of phosphorous, the pattern was changed from crystalline to amorphous. It has been reported that nickel phosphide (Ni_xP_y) diffraction peaks are observed in the same range as that of aluminum (38° , 44° , 65° , 78°) [16]. For this reason the intensity of crystallographic peaks of Ni-P layer is less intense. Fig. 3c corresponds to electroless nickel coating after heat treatment at 500°C during 1 h. New crystallographic peaks are observed corresponding to nickel/aluminum alloy formed at the interface due to the heat treatment [22]. Fig. 3d shows peaks of gold layer, which are very characteristic of a crystalline material, because the surface is completely covered, it is not possible to observe the Ni-P peaks.

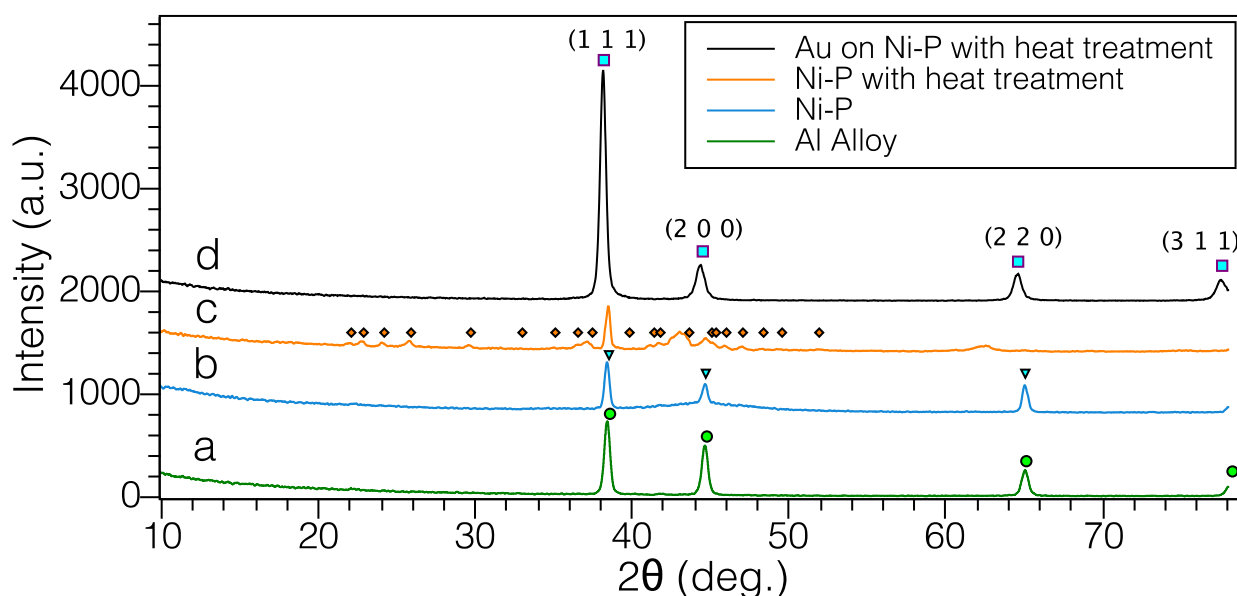


Figure 3. X-ray diffraction patterns of (a) AA6061 substrate, (b) Ni-P on AA6061, (c) AA6061 on Ni-P with heat treatment, (d) Au on Ni-P/Al6061 with heat treatment

Figs. 3c and 3b are shown in fig. 4 to compare the electroless nickel coating with and without heat treatment. Figure 4 reveals that with heat treatment the deposited Ni-P alloy has a mixed structure composed of an amorphous and some crystalline particles distributed in the matrix (Ni_3P , and Ni_5P_2 phases). The changes in structure, composition and improvement in mechanical properties due to the heat treatment are evidently observed with the annealed Ni-P deposit and results in the formation of

intermetallic precipitates in the deposit, such as Ni_3P and Ni_5P_2 phases. The intermetallic compounds with ordered structures cause the effect of precipitation hardening [14].

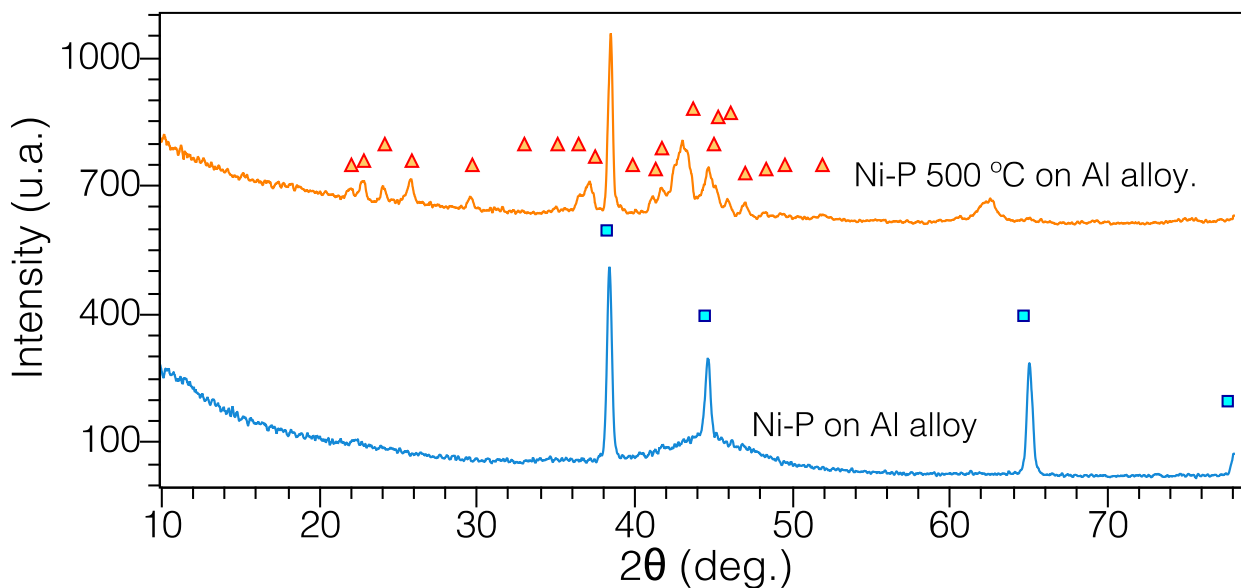


Figure 4. X-ray diffraction patterns of Ni-P deposit on aluminum substrate without and with heat treatment.

3.4 SEM

It was carried out the scanning electron microscopy analysis (fig. 5) to know the behavior of the Ni-P layer on aluminum before and after heat treatment and Au coatings on AA6061/Ni-P with heat treatment. In figure 5a it is observed a compact and uniform deposit with homogeneous grain size for the Ni-P on aluminum. When AA6061/Ni-P is thermally treated during 1 hour under nitrogen atmosphere (fig. 5b) the coating is more compact with respect to AA6061/Ni-P without heat treatment (fig. 5a). XRD studies discarded the presence of nickel oxide. On the other hand, gold coating on AA6061/Ni-P is a homogenous layer with lower roughness than Ni-P layer. The heat treatment improved the adherence of gold coating. Thickness of Ni-P coating was 2.5 μm and 100 nm for the gold layer.

XRD studies showed the effect of temperature. It is also possible to observe them in SEM images. Studies on stainless steel have shown that the thermal treatment at 400 °C improves the hardness value of the N-P coating due to the important grain-boundary density (precipitation of the Ni_3P phase). In addition, by increasing the temperature to 600 °C the sample has the highest bonding to the substrate [23]. For that reason, at 500 °C a good adhesion was obtained and the grains were more compact, which agrees with the results obtained.

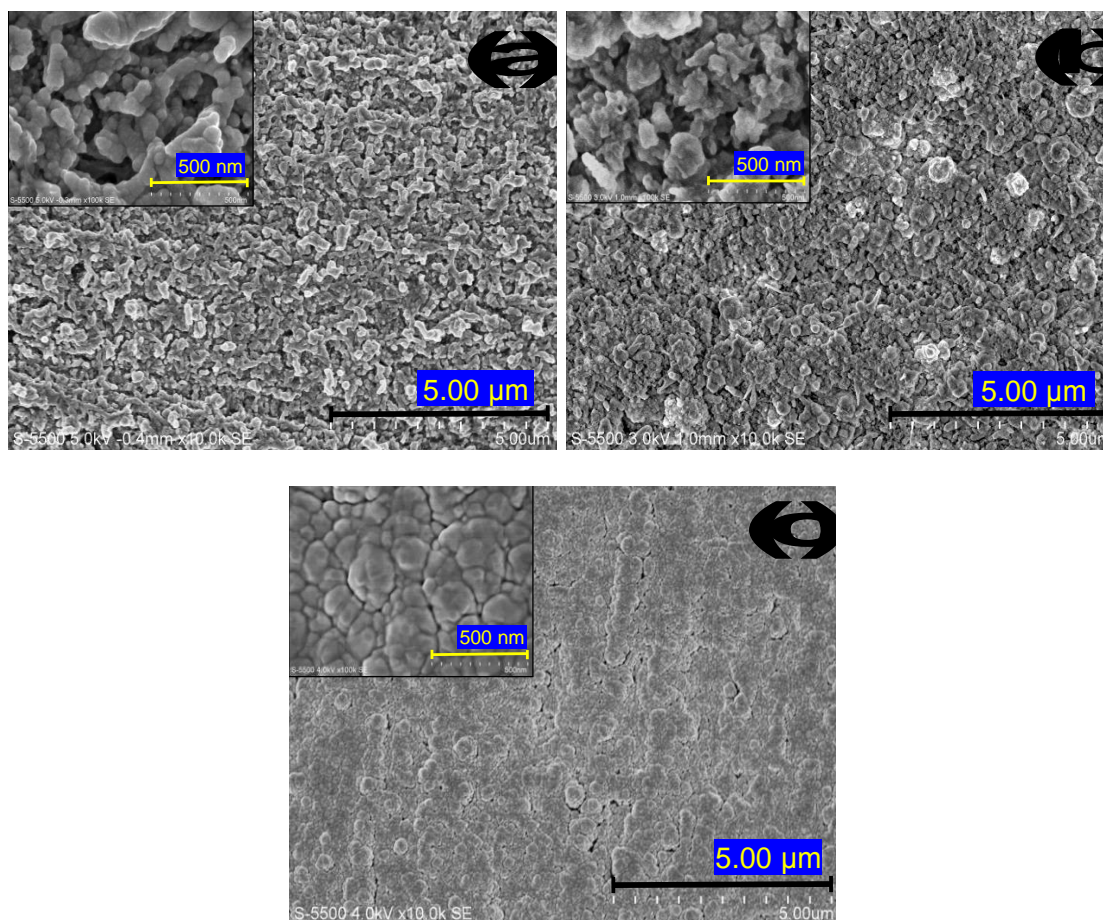


Figure 5. SEM of (a) Ni-P on Al alloy without heat treatment, (b) Ni-P on Al alloy with heat treatment and (c) Au on Ni-P with heat treatment.

3.5 Electrochemical Studies

Corrosion studies were conducted in $0.5 \text{ mol L}^{-1} \text{ H}_2\text{SO}_4$ (electrolyte). The solution was purged with oxygen or hydrogen gases to simulate a cathodic or anodic environment respectively. Figure 6 shows the open circuit potential (OCP) measured during 4 hours on bare AA6061 and AA6061/Ni-P/Au samples.

For each environment, the highest E_{OC} values were observed for Au on Ni-P with heat treatment. These open circuit potentials are stable for all cases. There is no formation of pores or passivation on the surface [22]. Comparison of corrosion current densities (I_{corr}) of uncoated aluminum and coated aluminum is shown in figure 7. A high corrosion potential (E_{corr}) and low corrosion current (I_{corr}) indicate that the material is resistant to corrosion. The Au on Ni-P with heat treatment showed a lower I_{corr} value ($5.26 \mu\text{Acm}^{-2}$) than Al alloy ($51 \mu\text{Acm}^{-2}$). The corrosion potential of the coated aluminum shifts towards more positive values compared to the uncoated aluminum. A thin layer of aluminum oxide is formed which protects it against corrosion [24].

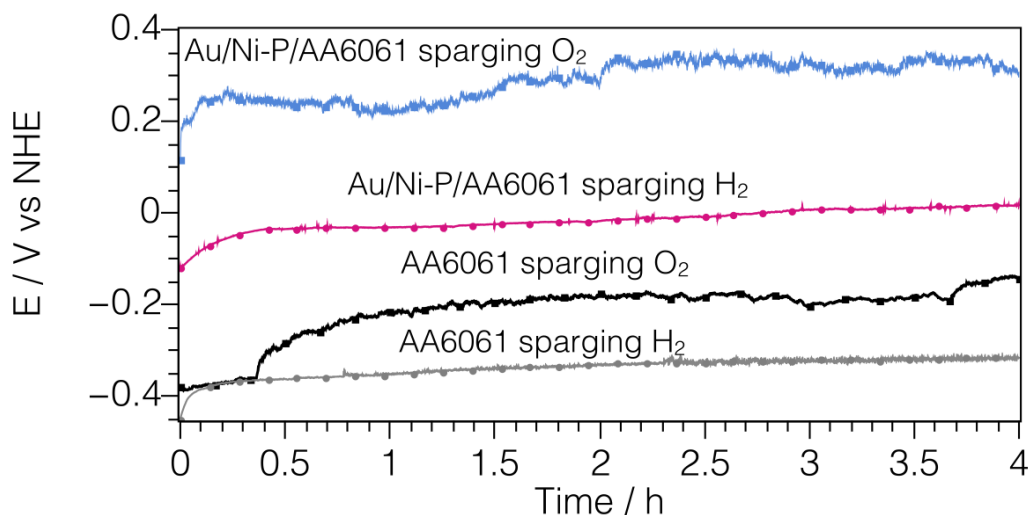


Figure 6. Open circuit potential evolution for 4 hours for bare AA6061 and Au/Ni-P/AA6061 with heat treatment, sparging O₂ and H₂ simulate cathode and anode respectively.

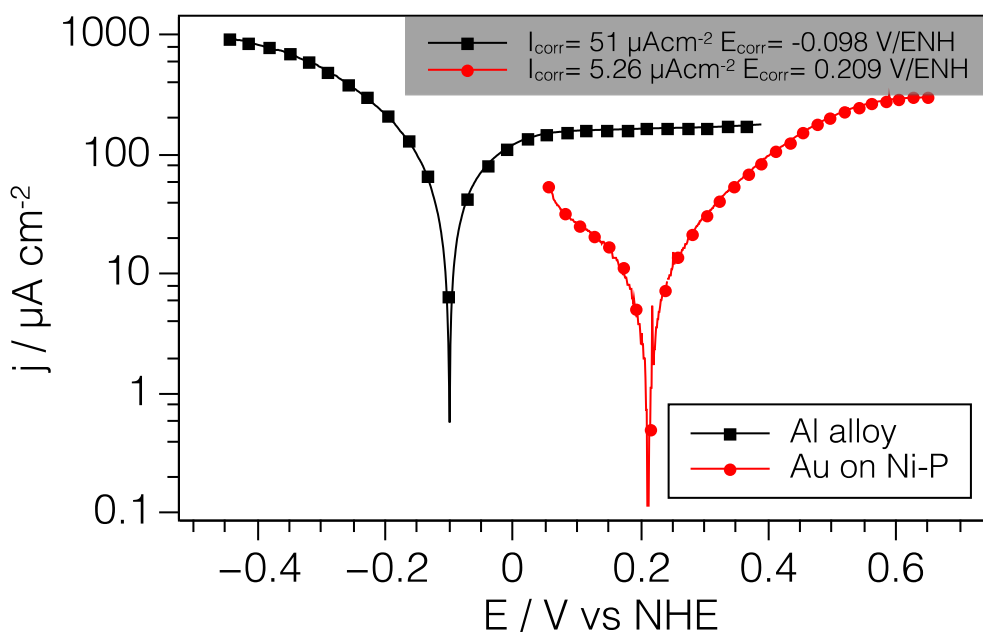


Figure 7. Potentiodynamic polarization curves for bare Al alloy and Au/Ni-P with heat treatment for samples in $0.5 \text{ mol L}^{-1} \text{ H}_2\text{SO}_4$.

An alternative for the deposition of gold is by electrolytic techniques. However, the use of toxic reagents is necessary. Electroless nickel immersion of gold (ENIG) process is one of the most used for gold deposition. In this method it has been found OCP values similar to those of this work, but with a much higher corrosion ($0.01 - 0.1 \text{ mAcm}^{-2}$), approximately two orders of magnitude higher compared to this work ($5 \mu\text{Acm}^{-2}$) [25].

4. CONCLUSIONS

In this study the AA6061 alloy was characterized with respect to its protection against corrosion by applying a Ni-P/Au layer for its possible application as bipolar plate in PEM fuel cell. The adhesion of the nickel deposit was improved with heat treatment at 400 °C for 1 hour, due to the formation of a solid solution between aluminum and nickel, which could be corroborated by XRD studies. A low amount of oxygen allowed improvement in adhesion and a better coating. The roughness of Ni-P layer enhances the adherence between the substrate and the PVD deposited gold coating. Zincating process promotes the nickel deposition on aluminum and protects it against corrosion. During this process roughness of zinc layer increased with time, hence zinc layer thickness has direct influence on the Ni-P layer. Electrochemical tests showed that the corrosion resistance improved by an order of magnitude (51 to 5 μAcm^{-2}) by employing Ni-P / Au coating. The open circuit potential was monitored for 4 hours by bubbling H₂ / O₂ in which stability of the sample was observed.

ACKNOWLEDGEMENTS

The authors wish to thank Maria Luisa Ramon Garcia and Gildardo Casarubias for their technical support in XRD and SEM-EDS measurements respectively.

References

1. E. Dur, Ö. N. Cora, M. Koç, *Journal of Power Sources*, 196 (2011) 1235.
2. J. Barranco, F. Barreras, A. Lozano, A. M. Lopez, V. Roda, J. Martin, M. Maza, G. G. Fuentes, E. Almandoz, *International Journal of Hydrogen Energy*, 35 (2010) 11489.
3. Y. Hung, H. Tawfik, D. Mahajan, *Journal of Power Sources*, 186 (2009) 123.
4. H. Tawfik, Y. Hung, D. Mahajan, *Polymer Electrolyte Fuel Cell Degradation*, Elsevier (2012) 249.
5. R. C. Makkus, A. H. Janssen, F. A. de Bruijn, R. K. A. Mallant, *Journal of Power Sources*, 86 (2000) 274.
6. S. Joseph, J. C. McClure, P. J. Sebastian, J. Moreira, E. Valenzuela, *Journal of Power Sources*, 177 (2008) 161.
7. E. Rhaïem, T. Bouraoui, F. Elhalouani, *IOP Conference Series: Materials Science and Engineering*, 13 (2010) p. 012038.
8. S. -Y. Tsai, C.-Y. Bai, C.-H. Lin, G.-N. Shi, K.-H. Hou, Y.-M. Liu, M.-D. Ger, *Journal of Power Sources*, 214 (2012) 51.
9. C. -H. Lin, S. -Y. Tsai, *Applied Energy*, 100 (2012) 87.
10. A. E. Fetohi, R. M. Abdel Hameed, K. M. El-Khatib, E. R. Souaya, *International Journal of Hydrogen Energy*, 37 (2012) 7677.
11. A. E. Fetohi, R. M. Abdel Hameed, K. M. El-Khatib, E. R. Souaya, *International Journal of Hydrogen Energy*, 37 (2012) 10807.
12. S. A. A. El-Enin, O. E. Abdel-Salam, H. El-Abd, A. M. Amin, *J. Power Sources*, 177 (2008) 131.
13. T. W. Jappes, B. Ramamoorthy, P. K. Nair, *Journal of Materials Processing Technology*, 169 (2005) 308.
14. C. -Y. Bai, Y.-H. Chou, C.-L. Chao, S.-J. Lee, M.-D. Ger, *Journal of Power Sources*, 183 (2008) 174.

15. E. Rudnik, T. Jucha, L. Burzynska, K. Cwięka, *Materials Science Forum*, 690 (2011)377.
16. E. Khan, C. F. Oduoza, T. Pearson, *Journal of Applied Electrochemistry*, 37 (2007) 1375.
17. K. Murakami, M. Hino, R. Furukawa, T. Kanadani, *Materials Transactions*, 51 (2010) 78.
18. R. Kang, Z. Peng, B. Liu, D. Wang, J. Liang. *Surface & Coatings Technology*. 309 (2017) 67.
19. C.-H. Lin, *Applied Energy*, 104 (2013) 898.
20. F. Delaunois, P. Lienard, *Surface and Coatings Technology*, 160 (2002) 239.
21. S. Court, C. Kerr, C. Ponce de León, J. R. Smith, B. D. Barker, F. C. Walsh, *Transactions of the IMF*, 95 (2017) 97.
22. J. M Guilermany, M. Torrel, S. Dosta, J. R. Miguel, *Revista de metalurgia*, 44 (2008) 317.
23. H. Bouaziz, O. Brinza, N. Haddar, M. Gasperini, M. Feki. *Materials Characterization*, 123 (2017) 106.
24. T. Chiang, A. Su, L. Tsai, H. H. Sheu, Ch. Lu, *Int. J. Electrochem. Sci.*, 9 (2014) 5850.
25. A. Accogli, A. Lucotti, L. Magagnin. *ECS Transactions*, 75 (2017)1

© 2018 The Authors. Published by ESG (www.electrochemsci.org). This article is an open access article distributed under the terms and conditions of the Creative Commons Attribution license (<http://creativecommons.org/licenses/by/4.0/>).